Optimization of Temperature-Dependent Optoelectronic Characteristics of Polycrystalline SnO_2/Si Hetero-junction Structure

Mahdi S. Edan

Directory of Quality Assurance and International Accreditation, Ministry of Higher Education and Scientific Research, Baghdad, Iraq

Abstract

In this work, polycrystalline tin oxide thin films were prepared and studied in order to fabricate heterojunctions by growing them on n-type silicon substrates. The electrical measurements on the prepared samples were performed at different substrate and annealing temperatures. The results of these measurements showed good uniformity of these films throughout the current-voltage characteristics in both forward and reverse bias conditions at different annealing temperatures. They showed that the I-V characteristics were highly improved by thermal annealing. The reflectivity and internal quantum efficiency of the SnO_2/Si were measured as functions of the incident light wavelength. As well, the short-circuit current density and open-circuit voltage were measured as functions of the incident light intensity. These measurements showed good optoelectronic characteristics of the fabricated structures stimulating to optimize their employment in solar cell applications. In addition, the low-cost production of such structures makes them very good candidates for solar energy conversion systems as cheap alternative energy techniques.

Keywords: (optoelectronic characteristics, thin films, SnO2/Si Heterojunction, solar cells)

Introduction

Metallic oxide semiconductors have attracted an intense interest in optoelectronic applications during the last two decades. Among them, tin oxide (SnO_2) was the subject of too many research works due to its characteristic features, especially the variation of band gap within

3.6-4.2 eV. This variation is mainly determined by the preparation method and the type of substrate [1]. Controlling the deposition conditions of SnO_2 films is an important step in controlling their electrical properties, facilitating the device design. Apart from the optical properties, it is of crucial importance to understand the charge transport processes in SnO_2. In this regard, the overall temperature behavior of the electrical conductivity can reveal the underlying charge transport mechanisms in this material [2]. The electron tunneling from the silicon conduction band into SnO_2 conduction band occurs at the participation of traps in the depletion region as shown in Fig. (1).

In this work, polycrystalline tin oxide (SnO_2) thin films were prepared to form heterojunctions on n-type silicon substrates and study their electrical characteristics as functions of the temperature and illumination.

Theortical Concept

For deep understanding of the conductivity behavior in the studied samples, it should be considered as a logarithmic derivation which is given by [3]:

$$W(T) = \left(\frac{T}{\sigma}\right)\frac{d\sigma}{dT} \qquad (1)$$

where $W(T)$ can be used to determine the metallic and insulating behaviors of conductivity

When the slope of plot between $\ln[W(T)]$ and $\ln T$ is negative, then the sample is considered as insulator, whereas the positive slope of the $W(T)$ plot indicates that the sample is considered as metal. On the other hand, in more detail, the decrease of $W(T)$ towards zero with decreasing temperature identifies the sample as a real metal, while the temperature-independent behavior of $W(T)$ indicates that the sample is weakly insulating [3].

In polycrystalline materials, a high density of defects is expected at the grain boundaries, which are often charged with majority carriers. The charged states at the grain boundaries create depleted regions and potential barriers, which provide resistance to the passage of carriers [4]. According to the grain boundaries model [5], an increase in the crystallite size (L)

causes a decrease in the grain boundaries scattering and this leads to a decrease in the surface trap density (N_t).

The relative internal quantum efficiency (IQE) of the fabricated cell is calculated according to the following equation:

$$IQE = \frac{hc}{q\lambda}\frac{1}{1-R_t}S_{R(\lambda)} \quad (2)$$

The IQE is a more fundamental quantity, which differs from EQE in the term (1-R_t), which accounts for reflection losses.

In solar cell construction, high film transmittance and conductivity are required in order to minimize the efficiency losses due to absorption of a part of the spectrum and the Ohmic drop in the oxide layer. The analysis of the system is based on considering the current density (J)-voltage (V) relationship as a function of the effective series resistance (R_s) according to the following [6]:

$$J = J_{ph} - J_0\, e^{T}([q/nkT(V + JR_s] - 1) \quad (3)$$

where J_{ph} is the photo-generated current density, J_o is the reverse saturation current density (=10^{-7} A.cm^{-2}), n is the diode quality factor (=1.6), and k, q, and T have their usual meaning

For the short-circuit conditions (V=0)

$$R_s = \frac{nkT}{qJ_{sc}} ln\left(\frac{J_{ph} - J_{sc} + J_0}{J_0}\right) \quad (4)$$

Experiment

Single crystal silicon substrates of (111) orientation, n-type conductivity, 1×1 cm^2 area, and a resistivity of (1.5-4) Ω.cm were used. In order to remove any residual oxides on these substrates, they were etched with (3:3:5) CP4 solution consisting of HNO_3, CH_3COOH, HF,

respectively. Then they were cleaned by alcohol and ultrasonic machine for 15 minutes then they were cleaned by water and ultrasonic waves for another 15 minutes.

High-purity tin (Sn) thin films were deposited on silicon substrates using thermal evaporation technique under vacuum pressure of 10^{-6} Torr. Tin oxide (SnO_2) films were obtained with aid of rapid thermal oxidation. For this purpose, a halogen lamp was used as the oxidation source under an oxidation condition of 600°C for 90s to form SnO_2 on the silicon substrates to produce TCO's/Si heterojunction. Ohmic contacts were fabricated by evaporating high-purity (99.999) aluminum wires for back contact and high-purity (99.999) gold was used as front contact using Edwards coating system. The reflectance of the fabricated SnO_2-(n)Si structure was measured using SP-H 1011 spectrophotometer.

Results and Discussion

Figure (2) shows ln[$W(T)$] vs. ln$T$ for the samples. The temperature-dependent $W(T)$ studies were carried out in the range of 60-200K for the samples at different deposition temperatures (T_d) as shown in Fig. (2). Here, therefore, the investigated samples exhibit metallic-like and weakly insulating behavior for T<100K and T>100 K, respectively.

The plot of ln($\square T$)$^{1/2}$ vs. $10^3/T$ for the samples with varying deposition temperature is shown in Fig. (3). The conductivity increases rapidly with increasing temperature from 100 to 200 K, and increases slowly below 100 K. The data show the presence of two different conduction mechanisms. One is the thermoionic emission through the grain boundaries, which has activation-type temperature dependence due to the carrier activation in the grain boundaries in the temperature range above 100 K, and the other is the tunneling below 100 K, in which the conductivity may be considered to be temperature independent. We believe that this residual temperature dependence of conductivity is due to the tunneling effect. It is well known that, unlike thermionic emission, the tunneling effect is independent of temperature [4]. In the case of tunneling carriers can overcome the depletion region by tunneling. If tunneling takes place between the top of the barrier and the Fermi level, the thermoionic emission occurs. In this case, when the barrier height is small, carriers can surmount the barrier [4,5].

As previously mentioned, the conductivity of our samples has an activated character, including two intervals with different slopes as can be observed from Fig. (3). This situation is consistent with the behavior of W given in Fig. (2). In Fig. (2), one can expect that the high-temperature slope (T>100 K) is connected to the thermoionic emission for the samples by the following equation [7]:

$$\sigma_{TE} = \left(\frac{Le^2 n v_c}{kT}\right) e^{\frac{E_b}{kT}} \quad (5)$$

where E_b is the barrier height

The crossover temperature between thermoionic emission and tunneling in the films is about 100 K. The conductivities progressively cross over to a very weakly temperature-dependent regime below 100K. A metallic-type regime with an essentially constant conductivity below 100 K is clearly found for all the samples. We believe that the physical origin of this behavior is related to the tunneling effects because of the polycrystalline nature of the films.

The electrical conductivity in the tunneling regime is given as [8]:

$$\sigma_{TN} = \left(\frac{Le^2\psi}{\hbar^2 l_2}\right) exp\left(-\frac{4\pi l_2 \psi}{h}\right) \quad (6)$$

where

$\psi = \sqrt{2m^* E_b}$, $l_2 = \sqrt{\frac{\varepsilon\varepsilon_0 E_b}{e^2 N_d}}$, l_2 is the depletion layer width, h is the Planck's constant, ε_0 is the dielectric constant of vacuum, ε (=11.65) is the static dielectric constant, and N_d is the donor concentration

The values of l_2 are calculated by fitting Eq. (6) to the low-temperature range shown in Fig. (3) and then the values of N_d are obtained. One can expect that the width of l_2 decreases with the increase in N_d, while the tunneling probability increases. As a consequence, the conductivity increases as the width of l_2 decreases. However, we should consider a combined

effect of N_d and l_2 on the conductivity of the investigated films as explained before. Figure (4) shows the variation of depletion layer width with the doping concentration at different barrier height energies (E_b).

The investigated films exhibit this expected behavior. The surface trap density (N_t) of the films was found to decrease with the increase in the deposition temperature. Trapping states are capable of trapping free carriers and, as a consequence, more free carriers become immobilized as the number of trapping states increase. There are two cases: either the depletion layer (l_2) extends throughout the crystallite, or only a part of the crystallite is depleted of carriers. In the latter case, the depletion layer width is smaller than the crystallite size (l_2<L) and the surface trap density is given as [4]:

$$N_t = \frac{\sqrt{8\varepsilon\varepsilon_0 N_d E_b}}{e} \qquad (7)$$

The SnO_2 films in this study satisfy the condition l_2<L. Utilizing Eq. (7), we can now calculate the values of N_t. The obtained N_t values agree well with the values of the surface state density for various polycrystalline systems [9,10].

This study indicated that T_d has an important effect on the electrical properties of the films. The conductivity of the films was found to increase with the increase in the deposition temperature from 400 to 500°C and then decrease with a further increase in the T_d. At 400°C, the conductivity is the lowest of the films and the conductivity decreases with T_d from 500 to 600°C. This effect is also confirmed from the values of the N_d. Knowing the values of l_2 and E_b, the values of N_d can be calculated as mentioned before. Note that N_d of the films increases with the increase in T_d from 400 to 500°C and then decrease with a further increase in T_d.

The I-V characteristics of the SnO_2/Si structure for a thickness of 500 nm are shown in Fig. (5). The dark forward I-V characteristic for the SnO_2-(n)Si structure were measured in the annealing temperature range 25-150°C, the SnO_2 thickness was 500nm. The independence of the slope of the forward branches of the I-V characteristics on the temperature is their

peculiarity. Such behavior of the forward current is characteristic for the case of tunnel processes.

The doping level of n-type Si ($10^{15}cm^{-3}$) is too small for direct tunneling through the barrier, and the electron tunneling from the silicon conduction band into SnO_2 conduction band occurs at the participation of traps in the depletion region [11]. Figure (6) shows the reverse I-V characteristics of the SnO_2-(n)Si structure at different annealing temperature.

For voltage less than 0.65 V, the reverse current is proportional to the voltage, but at voltage greater than 0.65 V, a sharp rise of current due to tunnel transition of electron from the conduction band of SnO_2 into the conduction band of Si is noticed. The reverse current is determined by the transport of the minority carries from the Si valance band to the SnO_2 conduction band for the small indirect bias up to 0.65 V. For large values of reverse voltage, the voltage drops due to the semiconductor and insulation film characteristics.

The photoelectric properties have been investigated at the illumination of the structures through the wide gap semiconductor (SnO_2). The short circuit current density depends on illumination intensity. The current starts increasing at □>0.5□m and the maximum current obtained at wavelength equal to 0.95□m.

The photosensitivity region of the SnO_2/Si heterojunction structures is limited by the photon energies [11], which correspond to the band gaps of SnO_2 and Si. The generation and separation of electron-hole pairs occurs only in silicon. Figure (7) shows the relation between reflectivity and the incident light wavelength for a wavelength between 0.3 to 1.1□m.

The reflectivity of the fabricated cell increases as the wavelength is moved toward the transmission region of silicon. It has a value of 0.4 at short wavelength while this value increases to about 0.57 at longer wavelength. The lower values of reflectivity can be attributed to the SnO_2 layer, which acts as an anti-reflecting coating as well as a transparent upper contact.

Figure (8) shows the relative IQE for the fabricated SnO_2-(n)Si structure with 500 nm thickness and at 150°C. It is clear that the IQE of the fabricated cell increases with the increasing of wavelength. The cell exhibit about 40% IQE at wavelength of up to 750 nm. The IQE start to increase at wavelength equal to 900 nm, and the maximum IQE value occurs at wavelength equal to 1050 nm. Practically, IQE approaches minimum value at long wavelength because of parasitic absorption losses, such as absorption in the rear reflector and free carrier absorption [3].

For all studied solar cells, the SnO_2 layers are almost of the same thickness, therefore R_s of the cell is then proportional to the film conductivity. According to Eq. (4), a film conductivity of >150 □$^{-1}$.cm^{-1} is necessary to eliminate (or reduce) limitations of short-circuit photocurrent flow by R_s [12]. Since the conductivity of the proposed samples is higher than this value (5xl0^3 □$^{-1}$.cm^{-1}), then the short-circuit current flow limitations shown in Fig. (9) may be attributed to absorption of a part of the spectrum in the barrier layer.

The analysis of the fill factor can be obtained by considering the slope of the J vs. V relation (Eq. 3) at the open-circuit potential (V_{oc})

$$V_{oc} = \left(\frac{dJ}{dV}\right)V = -\left[R_s + \frac{nkT}{J_0 q} exp\left(-\frac{qV_{oc}}{nkT}\right)\right]^{-1} \quad (8)$$

Considering different open-circuit potentials ranging between 0.45 and 0.6 V and an ideal situation of R_s=0 □□ a slope of -0.2 A cm^{-2} V^{-1} is obtained. The value of this slope indicates that there exists a range of R_s values which have nearly no effect on the short-circuit current but strongly affect the shape of the J-V characteristics and consequently the fill factor. It means that the fill factor is too much affected by the conductivity of the barrier layer.

The high conductivity of the films is reflected in an increase in the fill factor to the extent which overcomes short-circuit current limitation due to the decrease in the transmittance and also the decrease of the open-circuit potential. The decrease in the open-circuit potential is now easy to explain in terms of the increased bandgap energy of the barrier layer. The increase in the bandgap energy is accompanied by an outwards shift of the band edges of the

semiconducting SnO_2 layer and hence a decrease in the available junction potential (V_j) is expected. This decrease is reflected in a corresponding decrease in the measured open-circuit potential of the considered cell.

Conclusions

The results of these measurements showed good uniformity of these films throughout the current-voltage characteristics in both forward and reverse bias conditions at different annealing temperatures. They showed that the I-V characteristics were highly improved by thermal annealing. Measurements showed good optoelectronic characteristics of the fabricated structures stimulating to optimize their employment in solar cell applications. In addition, the low-cost production of such structures makes them very good candidates for solar energy conversion systems as cheap alternative energy techniques.

References

1. M.F. Al-Kadhemy, Inter. J. of Mater. Phys., 2(1) (2011) 87-93.
2. S.-J. Chang, T.-J. Hsueh, I-C. Chen, S.-F. Hsieh, S.-P. Chang, C.-L. Hsu, Y.-R. Lin, and B.-R. Huang, IEEE Trans. on Nanotechnol., 7(6) (2008) 754-759.
3. A.G. Zabrodskii and K. N. Zinoveva, Sov. Phys. JETP 59 (1984) 425.
4. J.Y. W. Seto, J. Appl. Phys., 46 (1975) 5247.
5. J.W. Orton and M. J. Powel, Rep. Prog. Phys. 43 (1980) 1263.
6. H.J. Hovel, in **"Semiconductors and Semimetals,"** Vol. 11, R.K. Willardson, Editor, p. 519, Academic Press, Inc., New York (1978).
7. S. Altındal, S. Karadeniz, N. Tugluoglu, A. Tataroglu, Solid State Electronics, 47 (2003) 1847-1854.
8. R. Holm, J. Appl. Phys., 22 (1951) 569.
9. M. Kimura, Jpn. J. Appl. Phys., 50 (2011) 03CB01.
10. C.W. Nahm, J. Alloys Compd., 505 (2010) 657.

11. N. Timonah, A. B. Soitah, A. C. Yang, and A. L. Sun, Mater. Sci. Semicond. Process., 13 (2010) 125.
12. O. Bierwagen, M. E. White, M.-Y. Tsai, T. Nagata, and J. S. Speck, Appl. Phys. Express, 2 (2009) 106502.

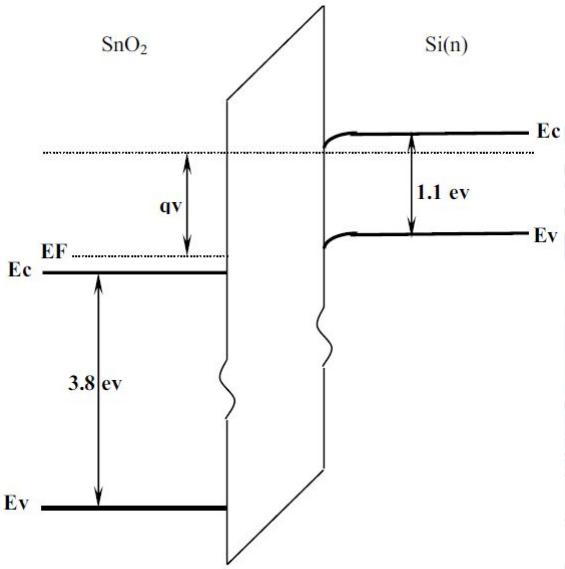

Fig. (1) The Energy band diagram at forward bias of SnO_2/Si structure

Optimization of Temperature-Dependent Optoelectronic Characteristics of Polycrystalline SnO_2/Si Hetero-junction Structure

Mahdi S. Edan

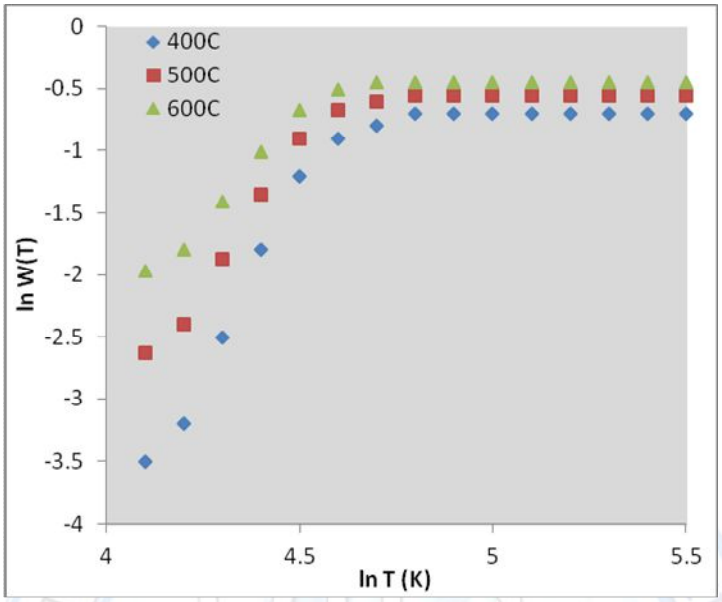

Fig. (2) Plot of ln[$W(T)$] vs. ln$T$

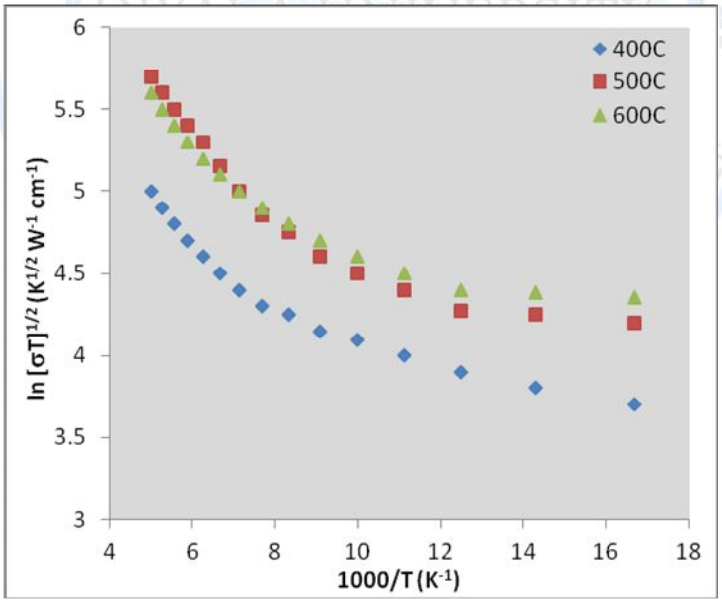

Fig. (3) Temperature dependence of the conductivity plotted as ln(σT)$^{1/2}$ vs. 1000/T

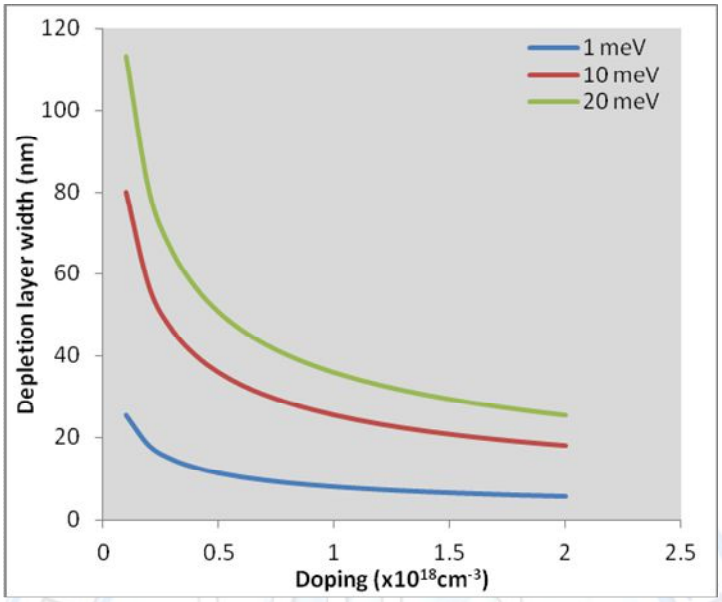

Fig. (4) Variation of depletion layer width (l_2) vs. doping concentration (N_d) at different barrier height energies (E_b)

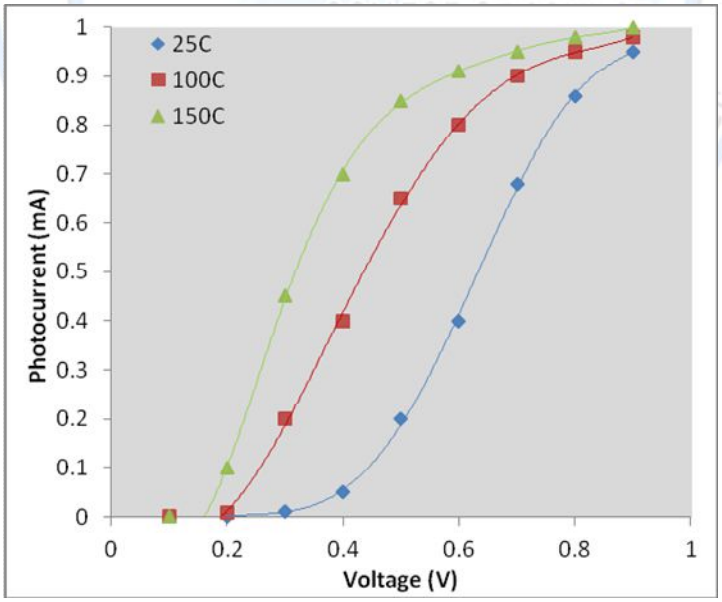

Fig. (5) The forward I-V characteristics of the SnO2/Si structure at different annealing temperature

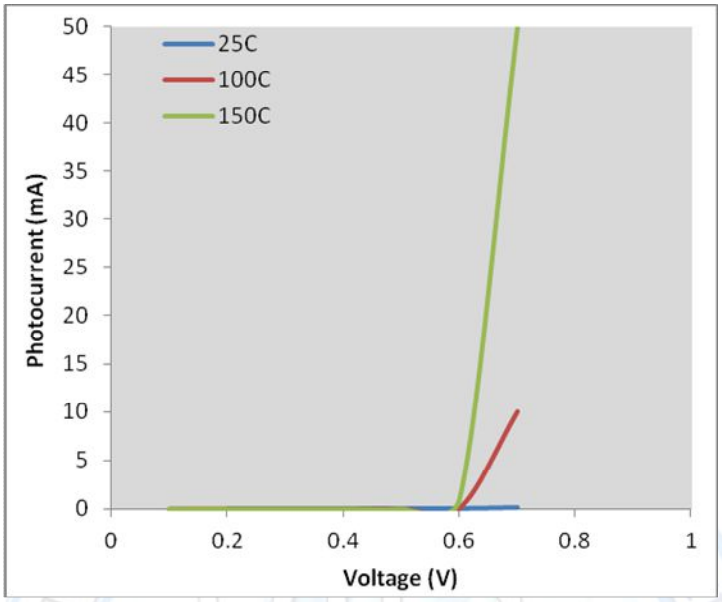

Fig. (6) The reverse I-V characteristics of the SnO_2/Si structures at different annealing temperature

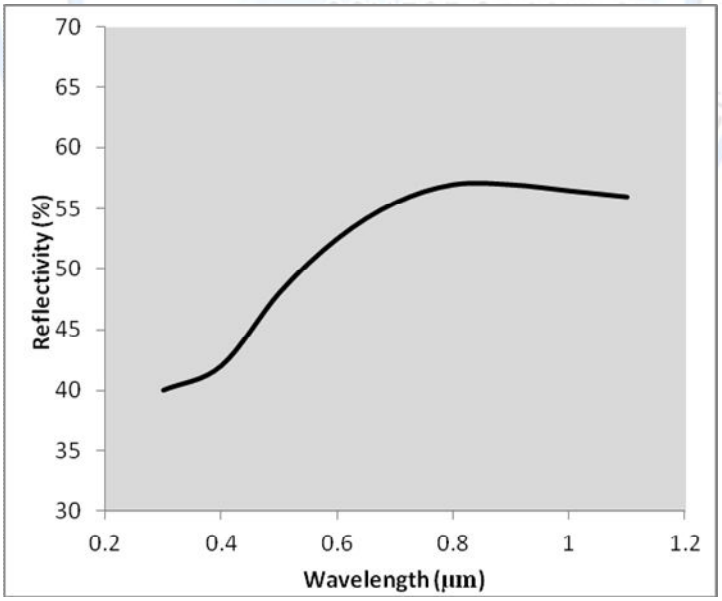

Fig. (7) Reflectivity vs. incident light wavelength

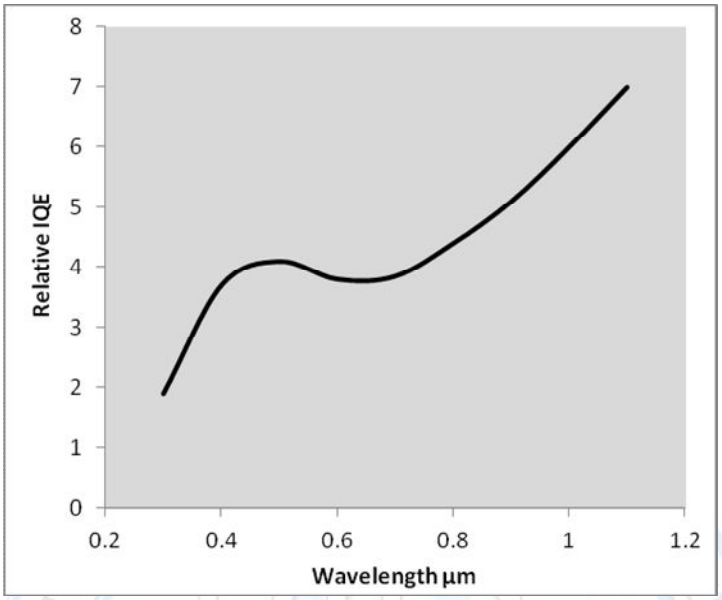

Fig. (8) Relative IQE vs. incident light wavelength for the fabricated SnO_2/ Si structure

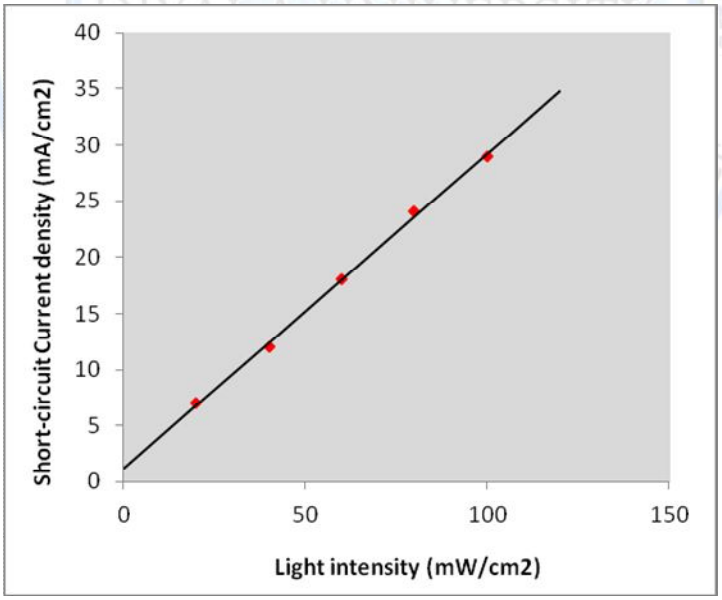

(a)

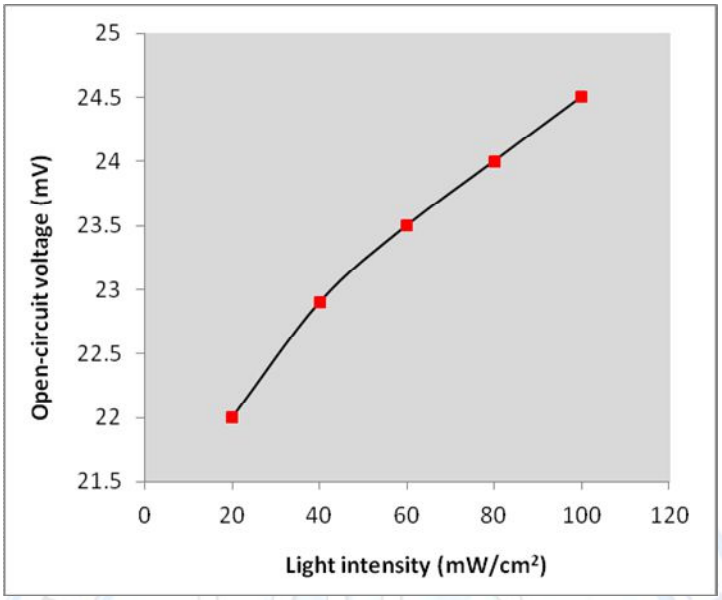

(b)

Fig. (9) Effect of incident light intensity on (a) the short-circuit current density (J_{sc}) and (b) open-circuit voltage (V_{oc}) of SnO_2/Si structure

Optimization of Temperature-Dependent Optoelectronic Characteristics of Polycrystalline SnO_2/Si Hetero-junction Structure

Mahdi S. Edan

تحسين الخصائص الكهروبصرية المعتمدة على درجة الحرارة للمفرق الهجين المكون من أوكسيد القصدير متعدد التبلور والسيليكون المانح

د. مهدي صالح عيدان

دائرة ضمان الجودة والاعتماد الدولي ، وزارة التعليم العالي والبحث العلمي، بغداد، العراق

الخلاصة

في هذا البحث، جرى تحضير أغشية رقيقة من أوكسيد القصدير متعدد التبلور ودراسة خصائصها ومن ثم تصنيع مفرق هجين من خلال ترسيبها على قواعد من السيليكون المانح. أنجزت القياسات الكهربائية على التراكيب المحضرة عند درجات حرارة مختلفة للقواعد وكذلك درجات حرارة تلدين مختلفة وقد أظهرت نتائج هذه القياسات انتظامية جيدة للأغشية المرسبة من خلال قياسات تيار-جهد بكلا حالتي الانحياز الأمامي والعكسي وعند درجات حرارة تلدين مختلفة، إذ ظهر أن خصائص تيار-جهد قد تحسنت بشكل ملحوظ نتيجة التلدين الحراري. جرى قياس الانعكاسية والكفاءة الكمية الداخلية للمفرق الهجين المصنع كدالة للطول الموجي الساقط على سطح المفرق الهجين. كما جرى قياس كثافة تيار الدائرة القصيرة وفولتية الدائرة المفتوحة كدالة لشدة الضوء الساقط على المفرق الهجين. وقد أظهرت هذه القياسات أن المفرق المصنع يمتلك خصائص كهروبصرية جيدة تشجع على استخدامه في تطبيقات الخلايا الشمسية. علاوة على ذلك، فإن انخفاض كلفة تصنيع مثل هذه التراكيب يجعلها مرشحة بشكل جيد للاستخدام في منظومات تحويل الطاقة الشمسية باعتبارها تقنية واطئة الكلفة للطاقة البديلة.

الكلمات المفتاحية: الخصائص البصرية, الأغشية الرقيقة ,اوكسيد القصدير, الخلايا الشمسية, المفرق الهجين.